ISSN 1063-7834, Physics of the Solid State, 2012, Vol. 54, No. 7, pp. 1388–1396. © Pleiades Publishing, Ltd., 2012.
Original Russian Text © V.S. Zhandun, V.I. Zinenko, 2012, published in Fizika Tverdogo Tela, 2012, Vol. 54, No. 7, pp. 1309–1316.

FERROELECTRICITY

Lattice Dynamics and the Ferroelectric and Antiferrodistorsive Instabilities in a Bulk Crystal and Thin Films of $SrZrO_3$

V. S. Zhandun* and V. I. Zinenko

Kirensky Institute of Physics, Siberian Branch of the Russian Academy of Sciences, Akademgorodok 50–38, Krasnoyarsk, 660036 Russia

** e-mail: jvc@iph.krasn.ru*

Received October 19, 2011; in final form, December 10, 2011

Abstract—The lattice dynamics and energies of phases related to antiferrodistorsive and ferroelectric distortions of bulk crystals and thin films of the $SrZrO_3$ crystal have been calculated within the framework of the ab initio model of an ionic crystal. In the case of a bulk crystal, it has been found that the most energetically favorable phases are related to antiferrodistorsive lattice distortions. Ferroelectricity in the $SrZrO_3$ crystal is suppressed by structural lattice distortions. In the case of thin films, it has been found that the ferroelectric instability is retained after the "rotation" of the oxygen octahedron and the film remains polar both in the case of a free surface and with the inclusion of the $SrTiO_3$ substrate in the calculation. The spontaneous polarization of thin films of different thicknesses in the ferroelectric phase has been calculated.

DOI: 10.1134/S1063783412070359

1. INTRODUCTION

Crystals of strontium zirconate $SrZrO_3$ belong to a large class of perovskite-like oxides with the formula ABO_3. However, in contrast to the majority of compounds with this chemical formula, which are fairly well understood, $SrZrO_3$ crystals have been studied in relatively few works [1–3], although a number of properties manifested by these materials make them suitable for various technological applications [4, 5]. It has also been found that, after doping with acceptors, these crystals begin to exhibit photon conductivity at high temperatures. This makes it possible to use strontium zirconate both in high-temperature technologies, such as fuel cells and high-temperature sensors, and in the process of electrolysis [5].

It is known that compounds with a perovskite-like structure can undergo both ferroelectric phase transitions (a typical representative is barium titanate $BaTiO_3$) and transitions associated with the rotation of the oxygen octahedron (a typical representative is strontium titanate $SrTiO_3$). According to the experimental data obtained by de Ligny and Richet [2], the $SrZrO_3$ crystal at high temperatures has a cubic perovskite unit cell (symmetry $Pm3m$) with the unit cell parameter $a = 4.1$ Å. With a decrease in the temperature, the crystal undergoes a sequence of structural phase transitions to the tetragonal phase $I4/mcm$, the orthorhombic phase $Cmcm$, and the orthorhombic phase $Pnma$ at temperatures of 1170, 830, and 700 K, respectively, and all these transitions are associated with rotations of the oxygen octahedra ZrO_6. Vali [6] performed the ab initio calculation with the ABINIT software package and demonstrated that the phonon spectrum of the cubic phase of the $SrZrO_3$ crystal exhibits only an antiferrodistorsive instability and that all the observed phase transitions are associated with the condensation of modes at the boundary points R and M of the Brillouin zone and with the joint action of the modes at the points R and M. According to the data obtained from experimental and theoretical investigations, no ferroelectric instability in this crystal has been observed. At the same time, it is known that the changeover from a bulk crystal to thin films, sometimes, leads to significant changes in the properties of the compound; in particular, there arises a ferroelectric state, as is the case, for example, with $SrTiO_3$ thin films, in which, as follows from the experimental data, there occurs a ferroelectric phase transition at a temperature of 304 K [7].

In this work, the high-frequency permittivities, Born effective charges, elastic constants, lattice dynamics, and energies of the phases related to the ferroelectric and antiferrodistorsive lattice distortions of the bulk crystal and thin films of the $SrZrO_3$ compound have been calculated within the framework of the ab initio model of an ionic crystal.

2. COMPUTATIONAL TECHNIQUE

The calculation was performed using the density functional theory method within the framework of the Gordon–Kim model for an ionic crystal with polarizable ions. Details of the model were described in the review by Maksimov et al. [8]. The calculation of the aforementioned parameters for the bulk $SrZrO_3$ crystal was carried out only for the cubic phase of this

compound (with the perovskite structure). The corresponding parameters for the thin films were calculated using the periodic geometry of the "slack" structure in which the surfaces were assumed to be free. In this model, the film is composed of periodically alternating layers of SrO and ZrO_2, which are surrounded by a vacuum layer in order to create periodic boundary conditions, as is shown in Fig. 1a. The number of layers determines the thickness of the film. The film thickness was varied from 3 to 15 layers (~4–30 Å). All the calculations were performed for the experimental value of the unit cell parameter (a = 4.1 Å). The $SrTiO_3$ substrate was taken into account also using the periodic geometry of the "slack" structure with allowance made for the vacuum, but a part of the ZrO_2 layer was replaced by the TiO_2 layers, as is shown in Fig. 1b, and the unit cell parameter of the film was chosen to be equal to the unit cell parameter of the substrate.

Since the ions in the film, especially the ions located in the vicinity of the surface, relax from their equilibrium positions in the ideal perovskite structure due to the presence of the surface, the equilibrium positions of the ions were determined according to the procedure of structure relaxation using the iterative method. To accomplish this, for each ion, we calculated the forces

$$f_j^\alpha = \frac{\partial E^{\text{tot}}}{\partial r_i^\alpha},$$

where E^{tot} is the total energy of the crystal, which is the sum of the contributions from the energies of the Coulomb interaction, the short-range interaction, and the dipole interaction: $E^{\text{Coulomb}} + E^{\text{short}} + E^{\text{dipole}}$. It should be noted that all the contributions to the total energy of the crystal in our model were described by the analytical expressions (see review [8]); therefore, the first derivative of the energy was not calculated by numerical differentiation, but it was also described by the analytical expressions, which could be easily obtained from the expression presented for the total energy in review [8]. Then, each ion was displaced in the direction of the forces acting on it; thereafter, the forces acting on the ions were again calculated, and the procedure was repeated until the forces at each ion exceeded the value of 2 meV/Å. After the relaxation, we calculated the limiting vibrational frequencies of the relaxed film.

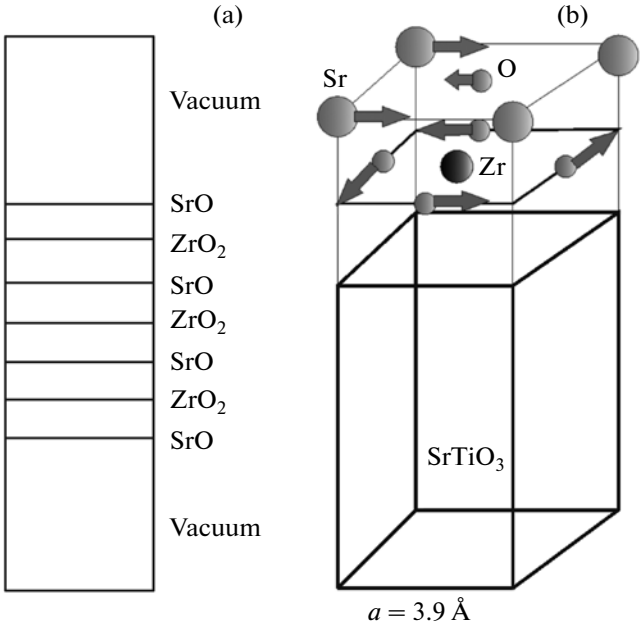

Fig. 1. Schematic representation of the periodic geometry of the "slack" structure for (a) the $SrZrO_3$ film with a free surface and (b) the $SrZrO_3$ film on a $SrTiO_3$ substrate.

3. RESULTS AND DISCUSSION

3.1. A Bulk $SrZrO_3$ Crystal

In the model described above, we have calculated the frequencies of lattice vibrations, Born dynamic charges, high-frequency permittivities, and elastic constants for the bulk $SrZrO_3$ crystal in the cubic phase. The calculated values of these parameters are presented in Table 1. Figure 2 shows the total phonon spectrum of the $SrZrO_3$ crystal in the cubic phase. It can be seen from this figure that, in the spectrum of lattice vibrations for this compound, there are strong instabilities at the M and R points of the Brillouin zone, which are responsible for the antiferrodistorsive instability of the crystal. It should be noted that, according to our calculations, in the vibrational spectrum of the crystal, there is also a ferroelectric instability. However, as can seen from Table 1, the absolute value of the frequency of the unstable ferroelectric mode is considerably smaller than the absolute values of the frequencies of the unstable antiferrodistorsive modes at the R and M points of the Brillouin zone, which are almost equal to each other. The eigenvectors of the antiferrodistorsive and ferroelectric modes are

Table 1. Calculated values of the limiting vibrational frequencies, high-frequency permittivities, Born dynamic charges, and elastic constants for the cubic phase of the bulk $SrZrO_3$ crystal

$\omega(q=0)$, cm^{-1}	$\omega(q=R)$, cm^{-1}	$\omega(q=M)$, cm^{-1}	ε	Z^*(Sr)	Z^*(Zr)	$Z^*(O_\perp)$	$Z^*(O_\parallel)$	C_{11}, GPa	C_{12}, GPa	C_{44}, GPa
60i	116i	110i	4.18	2.65	5.34	–4.4	–1.8	180	60	70

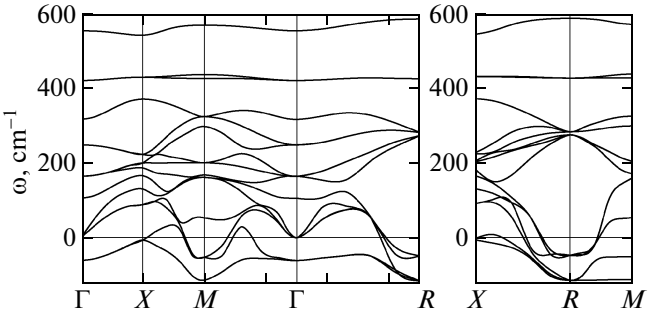

Fig. 2. Total phonon spectrum of the $SrZrO_3$ crystal in the cubic phase. Negative values of the frequencies correspond to unstable vibrational modes.

presented in Figs. 3a–3c. For the eigenvectors of the ferroelectric mode, the main displacements of the Sr and O ions occur in the direction perpendicular to the Zr–O bond ($\xi_{SR} = 0.81$, $\xi_{O\perp} = -0.42$, $\xi_{Zr} = 0.08$, $\xi_{O\parallel} = -0.07$). The eigenvectors of the modes at the *R* and *M* points of the Brillouin zone correspond to rotations of the oxygen octahedron ZrO_6. The distortions associated with the modes at the *R* point ($q = \pi/a(1, 1, 1)$) and at the *M* point ($q = \pi/a(1, 1, 0)$) will be designated as φ and ψ, respectively.

Table 2 presents the energies of the phases associated with the distortions of the crystal along the eigenvectors of the antiferrodistorsive and ferroelectric modes under consideration. The phase associated with the combination of distortions φφψ (symmetry *Pnma*) is found to be most energetically favorable. This phase is close in energy to the phases associated with the combinations of distortions φψψ (symmetry *Pnma*), φφφ (symmetry $R\bar{3}c$), 0φψ (symmetry *Cmcm*), and ψψψ (symmetry *Im*3), which is in agreement with the experimental data reported in [2]. As can be seen from Fig. 4a, the ferroelectric phase is also energetically favorable; however, in this case, the depth of the energy minimum, which is determined by the ferroelectric distortions, is two times smaller than that observed for the phase associated with the rotation of the oxygen octahedron. Figure 4b shows the dependences of the energies of the $SrZrO_3$ crystal on the amplitudes of the displacements of ions along the

Table 2. Energy difference between the cubic and antiferrodistorsive phases of the $SrZrO_3$ crystal (*Z* is the number of molecules per unit cell)

Distortion type	Symmetry group	$E - E_{cub}$, eV
φφψ	*Pnma* ($z = 2$)	−0.05
φφφ	$R\bar{3}c$ ($z = 1$)	−0.048
φψψ	*Pmmm* ($z = 4$)	−0.047
0φψ	*Cmcm* ($z = 2$)	−0.045
ψψψ	*Im*3 ($z = 4$)	−0.044

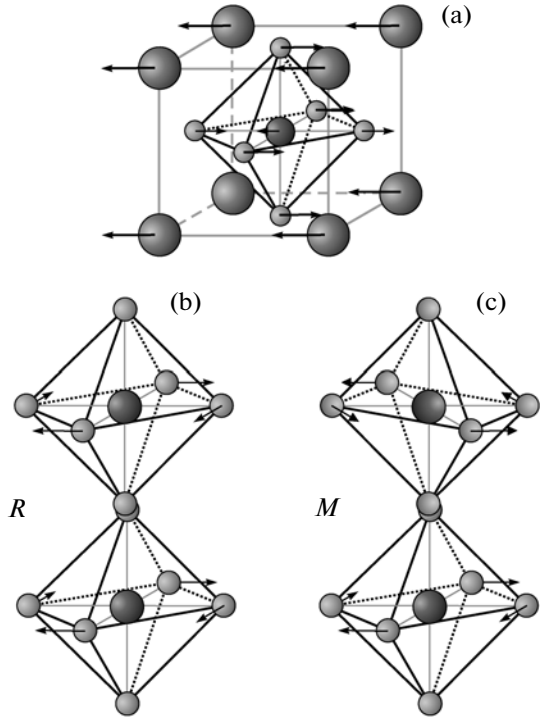

Fig. 3. Displacements of ions along the eigenvectors of the unstable modes: (a) the ferroelectric mode, (b) the R_{25} mode with the (φ00) distortion, and (c) the M_3 mode with the (00ψ) distortion. Designations of the atoms are the same as in Fig. 1b.

eigenvector of the ferroelectric mode in the phase where the oxygen octahedron is rotated through the angle corresponding to the energy minimum. It can be seen that the antiferrodistorsive lattice distortions completely suppress the ferroelectric instability.

Thus, it can be concluded that, in this compound, there exist phases associated with the rotation of the oxygen octahedron, whereas the ferroelectric state is not formed because of the suppression due to the rotation (curve *3* in Fig. 4b), which corresponds to the experimental situation.

3.2. $SrZrO_3$ Thin Films

The calculation of the aforementioned parameters for the $SrZrO_3$ thin films was performed using the above-described periodic geometry of the "slack" structure. Initially, for the films of different thicknesses, we carried out the procedure of structure relaxation in order to determine the equilibrium positions of the ions. The relative ion displacements obtained by the relaxation procedure for a seven-layer film used as an example are presented in Table 3 in comparison with the results of the calculation performed in [9]. As was expected, the ions located near the surface in the film undergo the largest displacements from the ideal positions of the perovskite structure.

In the relaxed structure, we calculated the high-frequency permittivities, Born dynamic charges, and frequencies of lattice vibrations at the boundary points Γ ($q = \pi/a(0, 0, 0)$) and M ($q = \pi/a(1, 1, 0)$) of the two-dimensional Brillouin zone. Figures 5a and 5b show the dependences of the calculated components of the high-frequency permittivity and the Born dynamic charges in the direction perpendicular to the plane of the film on the film thickness (the components in the direction parallel to the plane of the film remain almost unchanged with variations in the film thickness). With an increase in the film thickness, these quantities tend to the corresponding values for the bulk crystal. It should also be noted that the values of the dynamic charges on the surface appear to be larger in magnitude than the charges of the ions in the "volume" of the film. This circumstance is associated with the fact that the short-range dipole–charge interactions, which usually decrease the value of the dynamic charge in perovskites, for the surface ions are found to be smaller than those for the ions located in the "volume" of the film.

The most unstable frequencies of vibrations for the films of different thicknesses are presented in Table 4. It can be seen from this table that, in the vibrational spectra of the films of all the studied thicknesses, there is a ferroelectric mode, which is most unstable, and two less unstable modes associated with the rotation of the oxygen octahedron.

The eigenvectors of the "rotational" modes are presented in Figs. 6a and 6b. For the eigenvector of the most unstable antiferrodistorsive mode, the oxygen octahedra in the adjacent layers are rotated in the opposite directions (Fig. 6a), so that the magnitude of the ion displacements reaches the maximum in the center of the film and decreases toward the film surface. By analogy with the bulk crystal (Fig. 3b), distortions of this type will be referred to as the ψ distortions. In the second mode (Fig. 6b), the oxygen octahedra in the adjacent layers are rotated in the same direction and the magnitude of the ion displacements decreases from the maximum value on the surface of the film to the minimum value in the central layer. By analogy with the bulk crystal (Fig. 3a), distortions of this type will be referred to as the φ distortions. Also in the case where the layer containing the oxygen octahedron turns out to be the symmetry plane of the film, the vibrational spectrum contains the "rotational" mode, in which the ions located in the central layer remain immobile, whereas the layers located on the opposite sides from the center of the film are rotated in the opposite directions.

The dependences of the energy of the films of different thicknesses on the amplitude of the displacements of ions along the eigenvectors of the aforementioned antiferrodistorsive modes of the φ and ψ types described above are shown in Fig. 7. It can be seen from this figure that the rotation of the oxygen octahedron around the axis perpendicular to the film plane (displacements of the 00φ type) is most energetically favorable; in this case, the depth of the energy mini-

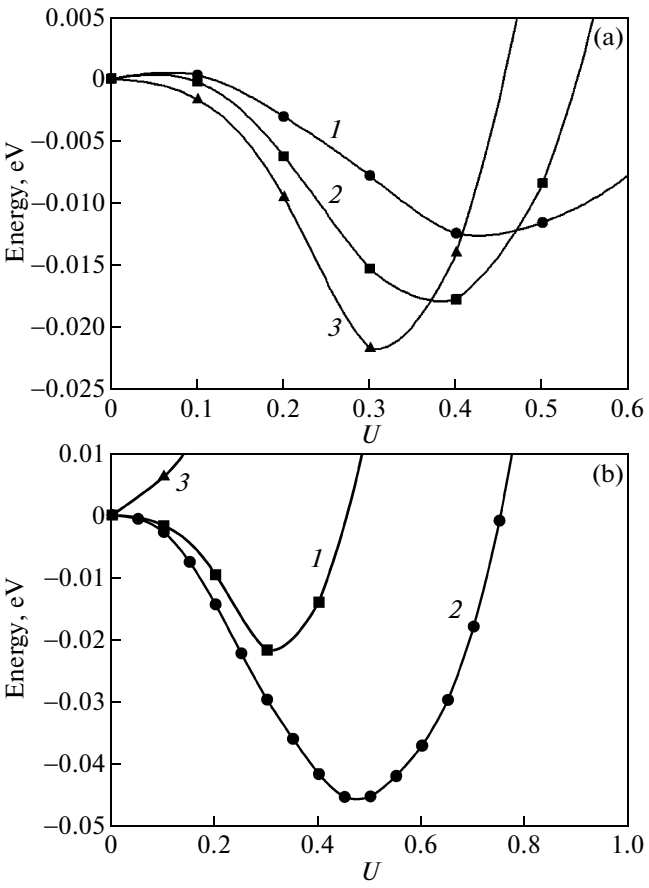

Fig. 4. (a) Dependences of the total energy of the crystal on the amplitude of the displacements of ions along the eigenvector of the ferroelectric mode in the directions (*1*) [100], (*2*) [110], and (*3*) [111]. (b) Dependences of the energies of the $\varphi\varphi\psi$ phase related to the rotation of the (*1*) oxygen octahedron, (*2*) ferroelectric phase, and (*3*) phase related to the ferroelectric distortions in the distorted antiferrodistorsive phase $\varphi\varphi\psi$ on the amplitude of the displacements of ions along the corresponding eigenvectors.

Table 3. Relative displacements of ions from the equilibrium position δ during the relaxation of a seven-layer film used as an example

Atom	δ, %	
	[9]	this work
Sr1	–7.63	–6.54
Sr2	–1.53	–1.81
Zr1	0.86	–1.86
O1(Sr)	–0.86	–4.70
O2(Sr)	–0.45	–1.20
O1(Zr)	–0.05	–1.70

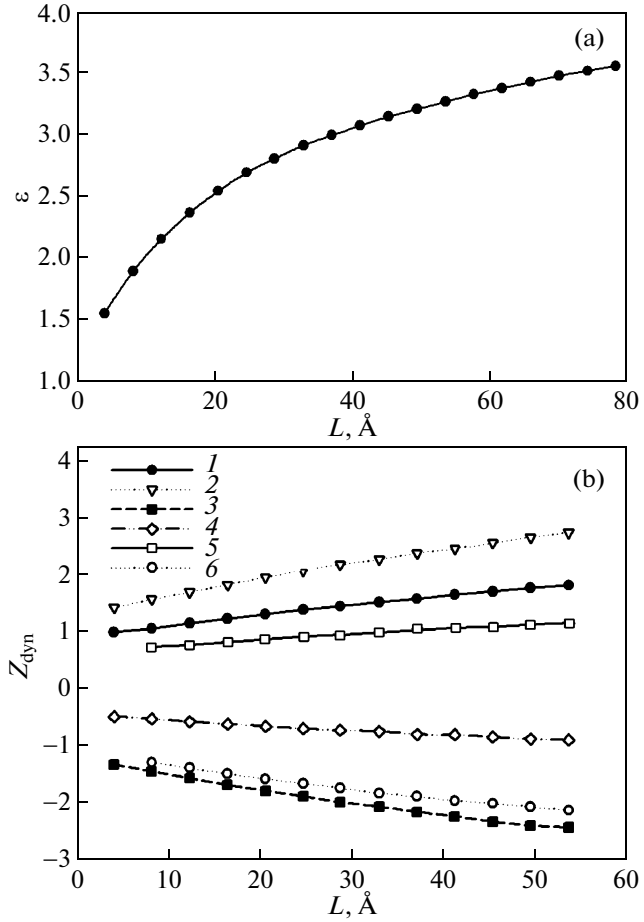

Fig. 5. Dependences of (a) the x components of the high-frequency permittivity ε and (b) the z components of the Born dynamic charges Z_{dyn} (in units of the charge e) on the film thickness L: (*1*) dynamic charge of the surface Sr ion, (*2*) dynamic charge of the Zr ion, (*3*) dynamic charge of the surface O ion located in the SrO plane, (*4*) dynamic charge of the O ion located in the ZrO_2 plane, (*5*) dynamic charge of the "bulk" Sr ion, and (*6*) dynamic charge of the "bulk" O ion located in the SrO plane.

mum drastically decreases with an increase in the film thickness. Table 5 presents the angles of rotation of the

Table 4. Unstable vibrational frequencies (in cm^{-1}) of the antiferrodistorsive and ferroelectric modes for the films of different thicknesses with a free surface

Mode	Number of layers						
	3	5	7	9	11	13	15
00ψ		99.1*i*	105.3*i*	109.8*i*	112.7*i*	114*i*	115*i*
00φ	104.5*i*	96.8*i*	98.7*i*	98.9*i*	99*i*	99.1*i*	99.1*i*
FE	134*i*	134.3*i*	134.6*i*	135*i*	135.3*i*	135.4*i*	135.5*i*

Note: Here and in the other tables, FE is the ferroelectric mode.

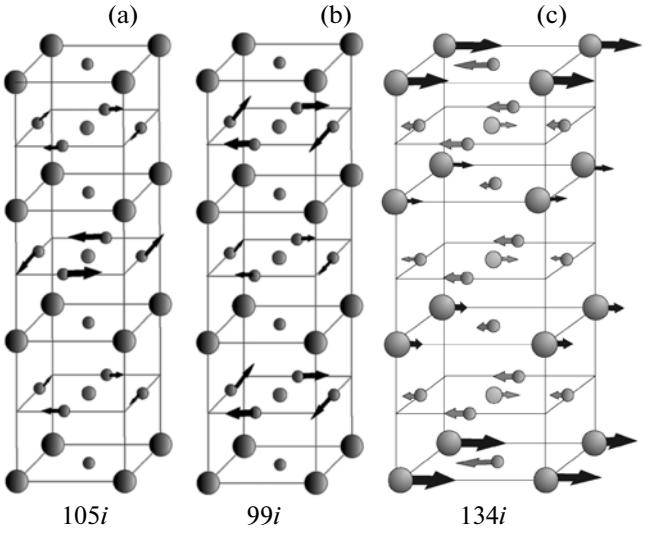

Fig. 6. Eigenvectors of the unstable modes related to rotations of the oxygen octahedra for the seven-layer film: (a) 00ψ distortions, (b) 00φ distortions, and (c) ferroelectric distortions. The relative displacements of the ions correspond to the sizes of arrows. Designations of the atoms are the same as in Fig. 1b.

oxygen octahedron, which correspond to the minimum energy for the 00φ and 00ψ distortions.

For the eigenvector of the ferroelectric mode, the Sr and O ions undergo the largest displacements, as is the case with the bulk crystal. It should also be noted that the largest magnitude of the displacements is found for the surface ions, and it decreases abruptly toward the center of the film, as is shown in Fig. 6c. The dependences of the total energy of the films of different thicknesses on the amplitude of the displacements of ions along the eigenvector of the ferroelectric mode are shown in Fig. 8a. The depth of the energy minimum also decreases with an increase in the film thickness; however, in this case, the ferroelectric phase appears to be much more energetically favorable than the phase associated with the rotation of the oxygen octahedron. Figure 8b shows the dependences of the total energy of the films distorted along the eigenvector of the ferroelectric mode in the phase corresponding to the rotation of the oxygen octahedron through a specific angle (Table 5). The results obtained from our calculations have demonstrated that, in the case of the thin films, antiferrodistorsive distortion do not suppress ferroelectricity, in contrast to the case of the bulk crystals, and the ferroelectric phase remains energetically favorable even after the rotation of the oxygen octahedron.

Using the obtained eigenvector of the ferroelectric modes, we calculated the spontaneous polarization of the films and the dependence of the spontaneous polarization on the film thickness. The calculated dependences of the spontaneous polarization of the

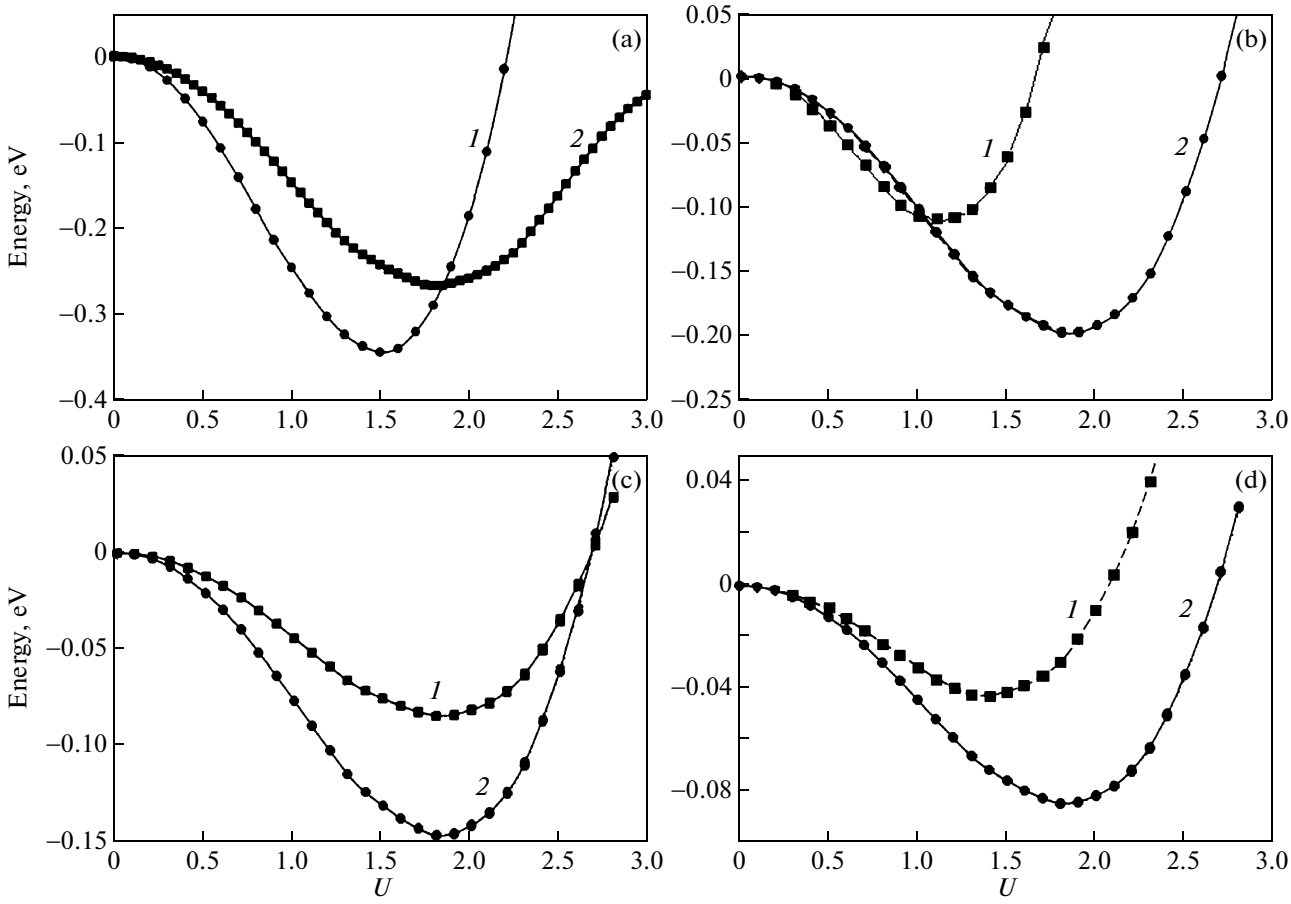

Fig. 7. Dependences of the energy of the films of different thicknesses on the amplitude of the displacements of ions along the eigenvectors of (a) antiferrodistorsive mode of the 00φ type for (*1*) three-layer film and (*2*) five-layer film and (b–d) antiferrodistorsive modes of the (*1*) 00ψ and (*2*) 00φ types for (b) seven-layer film, (c) nine-layer film, and (d) eleven-layer film.

thin films in the ferroelectric phase before and after the rotation of the oxygen octahedron are shown in Figs. 9a and 9b. It can be seen from these figures that, first, the spontaneous polarization reaches the maximum for the minimum thickness of the film and decreases with an increase in the film thickness, and, second, the spontaneous polarization in this case is considerably larger than the calculated value of the spontaneous polarization in the ferroelectric phase for the bulk crystal $P_S = 16.8$ μC/cm^2. It can also be seen that, although the spontaneous polarization decreases as a result of the antiferrodistorsive distortion of the structure of the film, it does not vanish and its value for the three-layer film is $P_S \approx 45$ μC/cm^2. Figure 9c shows the calculated polarization profile for the nine-layer $SrZrO_3$ film. The film appears to be polarized predominantly at the surface, so that the value of the polarization decreases abruptly deep into the film with an increase in the distance from the surface. This behavior of the polarization, for the most part, stems from the similar character of the eigenvector of the ferroelectric mode, because the dynamic charges vary only slightly from layer to layer.

3.3. Inclusion of the $SrTiO_3$ Substrate in the Calculation

The inclusion of the substrate in the calculation can lead to significant changes in the lattice dynamics and ferroelectric properties of thin films as compared to the film with free surfaces. This can be associated with the stresses generated in the film because of the mismatch between the lattice parameters of the film and the substrate, as well as with other factors (for example, with changes in the short-range interactions due to the replacement of the Zr ion by the ion Ti). In this regard, we calculated the lattice dynamics and energies of the $SrZrO_3$ thin films on the $SrTiO_3$ sub-

Table 5. Angles of rotation (in deg) of the oxygen octahedron for the films of different thicknesses

Mode	Number of layers				
	3	5	7	9	11
00φ	5.1	6.8	6.9	6.9	6.9
00ψ		6.8	1.4	1.1	1.0

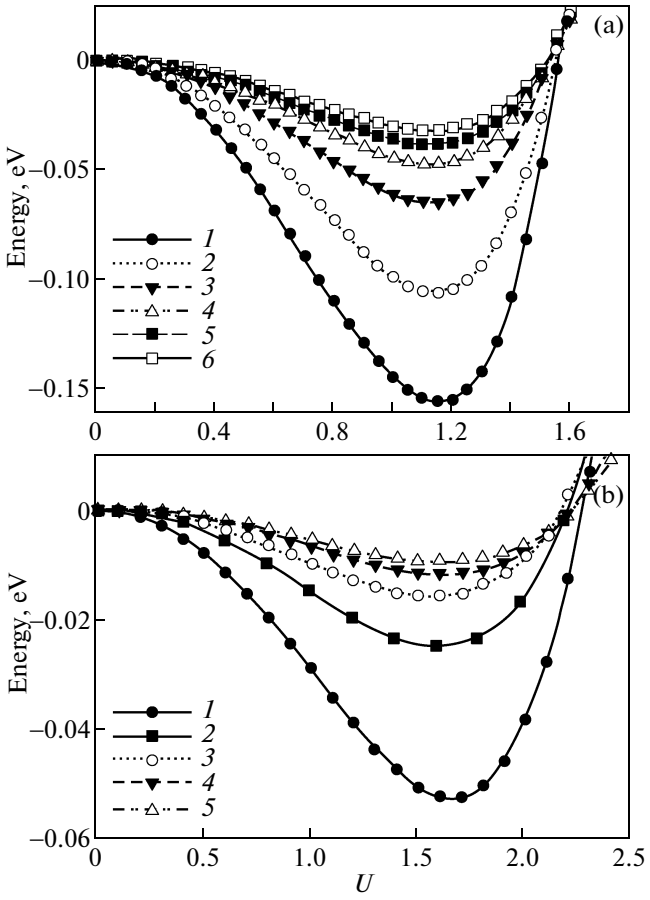

Fig. 8. Dependences of the total energy of the films of different thicknesses on the amplitude of the displacements of ions in (a) ferroelectric distortion and (b) ferroelectric distortions in the structure with a rotated oxygen octahedron for different numbers of layers: (*1*) 3, (*2*) 5, (*3*) 7, (*4*) 9, (*5*) 11, and (*6*) 13.

strate. For this calculation, we also used the periodic geometry of the "slack" structure with allowance made for the vacuum, as is shown in Fig. 1b. The thickness of the substrate was chosen to be equal to 19 monolayers, which made it possible to consider it as a continuum, and the thickness of the film was varied from 3 to 9 monolayers. The unit cell parameter of the film was chosen to be equal to the unit cell parameter of the substrate (a = 3.9 Å). Therefore, compressive stresses were generated in the film due to the mismatch between the lattice parameters of the film and the substrate, which was approximately equal to 5%. In this model, we calculated the limiting frequencies of lattice vibrations at the center of the two-dimensional Brillouin zone and at the boundary point M. The most unstable frequencies of lattice vibrations are presented in Table 6. It should be mentioned that the frequencies of lattice vibrations presented in this table are associated with the motion of ions of the film, whereas the ions of the substrate, as is evident from the eigenvector of these modes, remain immobile.

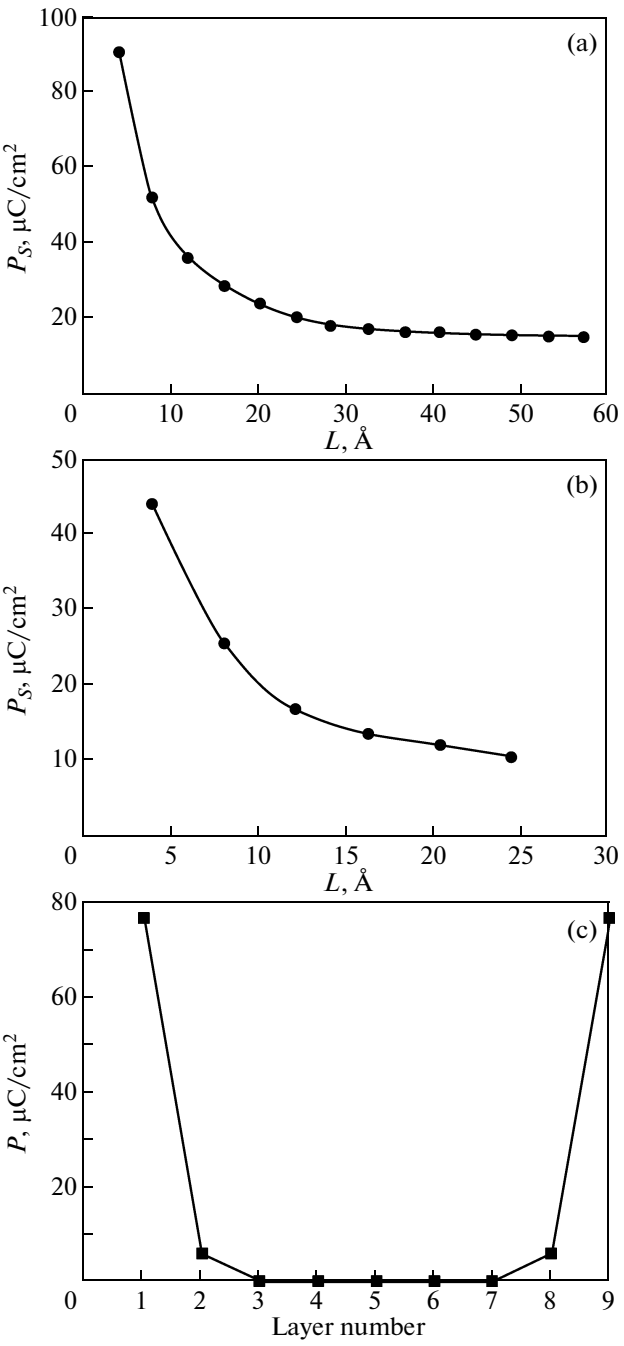

Fig. 9. (a, b) Dependences of the spontaneous polarization on the film thickness in (a) the ferroelectric phase and (b) the phase distorted along the eigenvector of the antiferrodistorsive mode and (c) the polarization profile for the nine-layer $SrZrO_3$ film.

A comparison of the data presented in Tables 4 and 6 has demonstrated, in the films under consideration, the ferroelectric instability is retained for all values of the film thickness, which, however, decreases in the absolute value of the frequency, whereas the unstable antiferrodistorsive modes, on the contrary, become significantly softer. Table 7 presents the energies of the

Table 6. Unstable vibrational frequencies (in cm^{-1}) of the antiferrodistorsive and ferroelectric modes for the films on $SrTiO_3$ substrates of different thicknesses

Mode	Number of layers			
	3	5	7	9
FE	104*i*	103*i*	102*i*	101*i*
00ψ	182*i*	186*i*	187*i*	188*i*
00φ		170*i*	174*i*	177*i*

Table 7. Energies of structures (in eV) associated with the distortions along the eigenvectors of the ferroelectric and "rotational" modes

Mode	$SrZrO_3$ film				$SrZrO_3$ film on the $SrTiO_3$ substrate			
	3 layers	5 layers	7 layers	9 layers	3 layers	5 layers	7 layers	9 layers
FE	−0.15	−0.10	−0.06	−0.05	−0.11	−0.07	−0.04	−0.03
00φ	−0.35	−0.27	−0.2	−0.15	−0.45	−0.31	−0.27	−0.22
00ψ		−0.27	−0.11	−0.08		−0.31	−0.2	−0.15
AFD + FE	−0.05	−0.02	−0.015	−0.012	−0.03	−0.01	−0.004	+0.006

Note: AFD + FE is the total distortion of the structure in two modes, namely, the antiferrodistorsive and ferroelectric modes.

ferroelectric and antiferrodistorsive phases, which were calculated for the $SrZrO_3$ film with inclusion of the substrate, in comparison with the energies of the same phases, which were obtained for the film with free surfaces. A comparison of these energies has demonstrated that, because of the influence of the stresses generated in the film, the ferroelectric phase becomes energetically less favorable, whereas the phase related to the antiferrodistorsive distortions 00φ becomes energetically more favorable. It should be noted that, upon rotation of the oxygen octahedron, the ferroelectric state persists only for the films with thicknesses from 3 to 7 monolayers and disappears for thicker films.

In the ferroelectric phase, we calculated the spontaneous polarization before and after the rotation of the oxygen octahedron. The obtained dependences of the spontaneous polarization on the thickness of the film are shown in Fig. 10. After the antiferrodistorsive distortion of the structure, the polarization is reduced by a factor of approximately two and, for the three-layer film, reaches ~26 μC/cm², which indicates the possible existence of a ferroelectric state in the $SrZrO_3$ thin films, in contrast to the bulk crystal, where it is suppressed by antiferrodistorsive distortions.

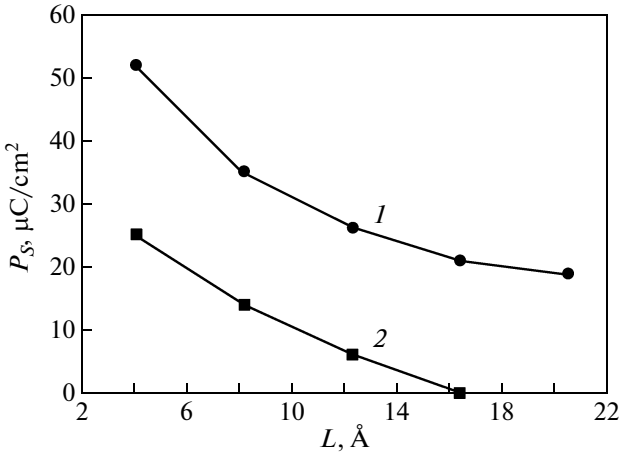

Fig. 10. Dependences of the spontaneous polarization on the film thickness in (*1*) the ferroelectric phase and (*2*) the phase distorted along the eigenvector of the antiferrodistorsive mode for a thin film on the $SrTiO_3$ substrate.

4. CONCLUSIONS

The main results obtained in this study can be summarized as follows.

The lattice vibrational frequencies, permittivities, elastic constants, and Born dynamic charges of the $SrZrO_3$ bulk crystal and thin films of different thicknesses have been calculated within the framework of the ab initio model of an ionic crystal. In both cases, the vibrational spectrum is characterized by two types of instabilities, namely, the antiferrodistorsive and ferroelectric instabilities. In the case of the bulk crystal, antiferrodistorsive distortions suppress the ferroelectric instability and the ferroelectric phase is not formed, which is consistent with the experimentally observed situation. In the case of thin films, antiferrodistorsive distortions only weaken the ferroelectric instability but do not suppress it completely, and the film remains polar down to a thickness equal to one

unit cell (the spontaneous polarization in this case is approximately equal to 45 $\mu C/cm^2$). The influence of compressive stresses associated with the substrate leads both to a decrease in the polarization induced in the film, as compared to the film with a free surface, and to the disappearance of this polarization at a film thickness of 9 monolayers in the structure with a rotated oxygen octahedron. The calculation of the polarization profile has demonstrated that the surface layers of the film are most strongly polarized, whereas the polarization of the inner layers is approximately equal to zero.

ACKNOWLEDGMENTS

This study was supported by the Russian Foundation for Basic Research (project no. 09-02-00067) and the Council on Grants from the President of the Russian Federation in Support of Leading Scientific Schools of the Russian Federation (grant no. NSh-4645.2010.2).

REFERENCES

1. E. Mete, R. Shaltaf, and S. Ellialtiouglu, Phys. Rev. B: Condens. Matter **68**, 035119 (2003).
2. D. de Ligny and P. Richet, Phys. Rev. B: Condens. Matter **53** (6), 3013 (1996).
3. C. J. Howard, K. S. Knight, B. J. Kennedy, and E. H. Kisi, J. Phys.: Condens. Matter **12**, 677 (2000).
4. C. Chen, W. Zhu, T. Yu, X. Chen, and X. Yao, Appl. Surf. Sci. **211**, 244 (2003).
5. T. Higuchi, T. Tsukamoto, S. Yamaguchi, N. Sata, K. Hiramoto, M. Ishigame, and S. Shin, Jpn. J. Appl. Phys. **41**, 6440 (2002).
6. R. Vali, J. Phys. Chem. Solids **69** (4), 876 (2008).
7. S. Davitadze, I. Shnaidshtein, F. Fadeev, B. Strukov, S. Shulman, B. Noheda, and A. H. G. Vlooswijk, Ferroelectrics **397**, 102 (2010).
8. E. G. Maksimov, V. I. Zinenko, and N. G. Zamkova, Phys.—Usp. **47** (11), 1075 (2004).
9. R. I. Eglitis and M. Rohlfing, J. Phys.: Condens. Matter **22**, 415901 (2010).

Translated by O. Borovik-Romanova